Letter

Chladni patterns explained by the space-dependent diffusion of bouncing grains

Anaïs Abramian,* Suzie Protière, and Arnaud Lazarus
Institut Jean le Rond d'Alembert, Sorbonne Université, CNRS, UMR 7190 Paris, France

Olivier Devauchelle
Institut de Physique du Globe de Paris, Université de Paris, CNRS, Paris, France

(Received 12 July 2024; revised 26 November 2024; accepted 11 April 2025; published 1 July 2025)

Although Chladni patterns are widely used to visualize the modes of vibration of an elastic plate, the mechanism by which the grains form the pattern is still debated. In this Letter, we suggest that the pattern results from space-dependent diffusion: grains gather where their diffusivity is low. We test this hypothesis in experiments, wherein we generate Chladni patterns on a vibrating membrane. We measure the diffusivity of the grains as a function of the vibration amplitude and propose an expression of the diffusive flux based on our measurements. We find a steady-state distribution of the grains in agreement with observations. These findings could inspire new methods to manipulate and segregate particles.

DOI: 10.1103/PhysRevResearch.7.L032001

When sand is sprinkled on a vibrating plate, the grains gather on the vibration nodes of the plate to form the famous Chladni patterns [1]. In this system, the grains behave as passive particles to visualize the plate's modes. These patterns have contributed to the development of the theory of elastic plates and are still used to design and tune the soundboard of musical instruments [2].

This phenomenon allows for the rapid and precise positioning of microscopic particles on a surface, including live cells, facilitating cell differentiation, tissue engineering, and the cultivation of multiple cell types [3]. Occasionally, in a liquid, micrometric particles concentrate in the antinodes, thus forming an inverse Chladni pattern [4]. Numerical simulations showed that, when the vibration acceleration is weaker than gravity, the grains can indeed be pushed towards the antinodes [5]. Similarly, fine powders can be sensitive to the air currents induced by vibrations and again driven towards the antinodes [6].

Overall, what pushes the grains towards the nodes in the classic experiment and, more broadly, what governs their motion remains an open question. A possible mechanism is that the grains, as they bounce on a tilted plate, feel a net force towards the nodes [5,7]. However, this explanation primarily applies to grains that slide or creep on the vibrated surface. Far from the bouncing threshold, a statistical approach becomes necessary and we need to consider the randomness of their motion to understand the formation of patterns [8]. This regime, which we investigate in this Letter, remains experimentally uncharted and a rigorous statistical theory describing this behavior has yet to be established. Our focus is specifically on dilute grain concentrations, where collisions between grains are negligible—unlike in previous studies [9–11].

In a recent experiment, Grabec [12] investigated how a single grain moves over a vibrating membrane. He showed that the jumps of the bouncing particle extend over a distance roughly proportional to the local vibration amplitude. This should result in a diffusivity D that varies over the membrane. However, the dependency of diffusivity on amplitude and frequency is elusive and the connection to the formation of a Chladni pattern remains to be established. Motivated by this question, we want to model the dynamics of a collection of grains bouncing over a vibrated membrane. To do so, we set up a Chladni experiment and track the particles therein. We find that their fluctuating trajectories are essentially random walks. This allows us to measure their diffusivity and its variation over the membrane. We suggest that this variation induces a heterogeneous grain density in steady state and we identify this heterogeneity with the Chladni figure. This new understanding could improve the controlled manipulation of particles over vibrated surfaces.

The experimental setup consists in clamping an elastomeric membrane of thickness 0.2 mm (ultrathin silicone sheet, Silex Ltd), initially without tension, between two rings. It is then stretched by placing a third rigid ring below the membrane [13]. The thickness of this additional ring controls the tension in the membrane. The radius of the clamped membrane is set at 13 cm. To prevent sticking, talcum powder is applied to the membrane before an experiment. The membrane and rings are fixed on a vertical shaker (Tira Vib 51140) excited by a sinusoidal signal of amplitude A and frequency $\omega/2\pi$ (Fig. 1).

To estimate the tension of the membrane, we measure the vibration amplitude of its center as a function of the shaking frequency, using a laser profilometer (Keyence LJ-V7060). Meanwhile, an accelerometer records the vibration of the frame (Brüel and Kjaer 4514). This reveals resonance

*Contact author: anais.abramian@upmc.fr

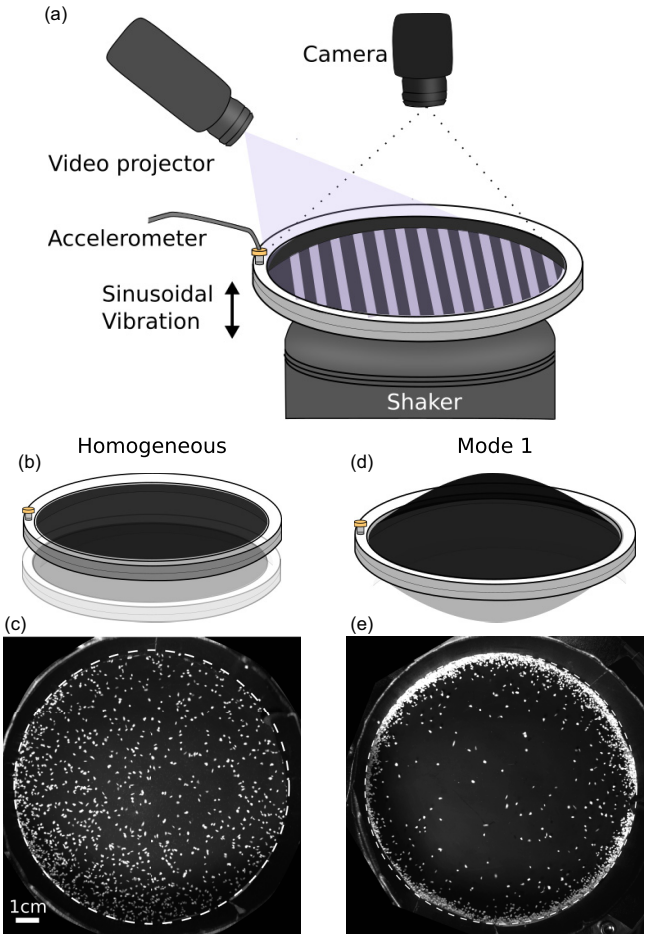

FIG. 1. (a) Experimental setup. A circular membrane is stretched over a ring and placed on a shaker. The vibration of the membrane is measured using fringe projection and Fourier Transform Profilometry. (b) Sketch of the membrane excited at a fixed amplitude and (c) corresponding experiment, seen from above. The amplitude of vibration and the grain concentration are homogeneous. See Movie 1 in the Supplemental Material. (d) Sketch of the membrane at the first mode of vibration and (e) corresponding experiment. The vibration is stronger in the center of the membrane and the grains gather along the ring. See Movie 2 in the Supplemental Material.

peaks which correspond to the classical modes of a circular membrane (Bessel functions). The resonance frequencies allow us to estimate the tension of the membrane ($T = 32 \pm 2$ N/m; see Supplemental Material). An inclined video projector (Qumi Q8), placed above the experiment projects a fringe pattern on the membrane in order to measure the vibration of the latter across its entire surface (Fig. 1).

To produce a Chladni pattern, we use rough plastic grains, of mean diameter $d = 830$ μm (blast media manufactured by Guyson). Sprinkling these grains over the membrane reveals the classical Chladni pattern, the two first modes being at $f_{01} = 73$ Hz and $f_{02} = 179$ Hz. As both the membrane and the forcing are axisymmetric, we observe only axisymmetric figures.

We start our investigation by tracking the grains' motion over a membrane that vibrates uniformly. This configuration, depicted in Fig. 1(b) and Movie 1, is achieved by fixing the frequency at 40 Hz, away from any resonant frequency. The grains randomly bounce in all directions and the overall concentration reaches a homogeneous steady state after a few seconds.

To characterize the grains' motion, we track their position over time and reconstruct their trajectory using the python library BrownTrack [14]. This library is based on the Munkres algorithm and facilitates the handling of a lot of trajectories (see Supplemental Material). Figure 2(a) shows a few trajectories over a membrane that vibrates uniformly. These trajectories appear to randomly explore the entire membrane. They resemble the trajectories of some bacteria, with alternating "runs," during which particles move along a straight path, and "tumbles," during which they undergo random reorientation [15]. In the present case, the runs correspond to jumps and tumbles to bouncing. The irregular shape of the grains causes the reorientation of the trajectory when the grain bounces (in contrast, glass beads tend to maintain their direction as they bounce).

As expected for a random walker, the average grain displacement vanishes, but the dispersion of the trajectories increases with time. To be quantitative, we define the root mean square displacement (RMSD) σ as

$$\sigma = \langle \sqrt{\langle [x(t+\tau) - x(t)]^2 + [y(t+\tau) - y(t)]^2 \rangle_t} \rangle_N, \quad (1)$$

where τ varies from zero to half the duration of a trajectory, $\langle \cdot \rangle_t$ the average over the duration of a trajectory, and $\langle \cdot \rangle_N$ indicates the ensemble mean over our set of trajectories. Figure 2(b) shows this quantity for a fixed membrane frequency (40 Hz) and different vibration amplitude A. For any amplitude, the data follow two regimes: a ballistic regime, where the RMSD is proportional to time, followed by a diffusive regime, where it is proportional to the square root of time. We are limited by the size of the circular membrane: when a grain hits the edge of the membrane, its trajectory ends. This explains why we do not have any measurement beyond $\sigma \sim 5$ cm. Although the transition between the two regimes is not sharp, it occurs after approximately 0.05 s, which is about twice the shaking period. Beyond this transition, one can measure the diffusivity; the next paragraphs are devoted to this measurement.

We now focus on the diffusive regime, which occurs after a few bounces. We measure the diffusivity D by fitting the relation $\sigma = \sqrt{4D\tau}$ to our observations [Fig. 2(b)]. For example, at $f = 40$ Hz and for an amplitude of $A = 0.29$ mm, we measure $D = 1.2 \pm 0.1$ cm^2/s. In other words, a particle typically needs one second to explore a square centimeter.

Varying the amplitude and the frequency, we report the diffusivity in Fig. 2(c). Diffusivity increases with amplitude at any frequency, but the grains begin to move only beyond a threshold, which we interpret as follows: for a grain to start bouncing, the membrane's acceleration $\omega^2 A$ needs to exceed that of gravity g. This interpretation suggests that the amplitude threshold varies with frequency according to g/ω^2, which closely match our observations [inset of Fig. 2(c)].

Because a bouncing grain follows a parabolic trajectory during each jump, we expect its diffusivity to be proportional to the horizontal component of its ballistic velocity v, defined as $\ell = v\tau$. If we neglect the friction of air, these parabola

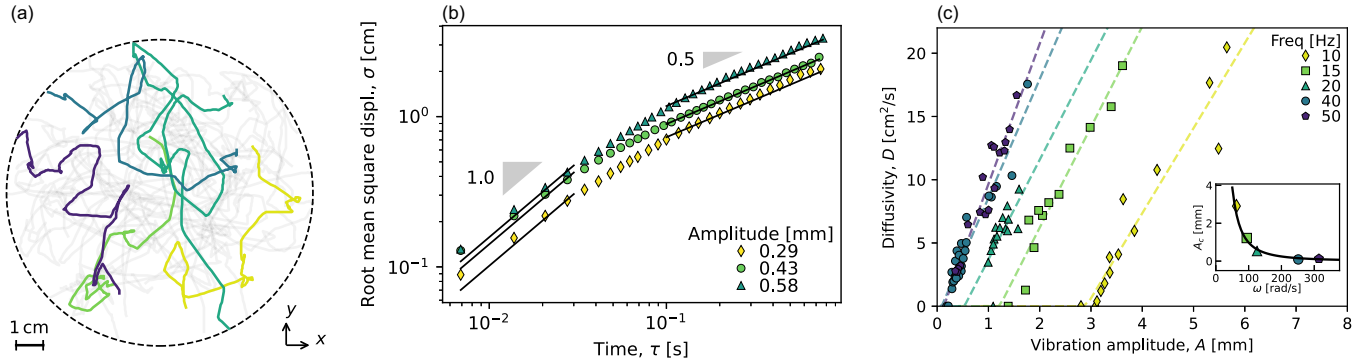

FIG. 2. (a) Grain trajectories, seen from above. The applied frequency is 40 Hz and the amplitude is 0.58 ± 0.02 mm. The dashed circle represents the edge of the membrane. (b) Root mean square displacement of the bouncing grains. Colors show the vibration amplitude for a fixed frequency of 40 Hz. These data reveal two regimes: ballistic (slope 1) and diffusive (slope 0.5). (c) Diffusivity as a function of the vibration amplitude for different frequencies. The colored lines are a linear fit for each frequency. Inset: amplitude threshold for bouncing at each frequency. The black line corresponds to $A_c = g/\omega^2$.

follow the equation $z(t) = -gt^2/2 + vt \tan\theta$, where θ is the angle at which the particle takes off, with respect to the horizontal. The length of a jump is thus $\ell = 2v^2 \tan\theta/g$ and, according to this simple model, the diffusivity reads

$$D \sim \ell^2/4\tau = \tan\theta \frac{v^3}{2g}. \tag{2}$$

The exponent of 3 compares well with our observations (black line, inset of Fig. 3). The fitted coefficient corresponds to an average rebound angle of 53°.

Once we have established a relationship between diffusivity and velocity, we need to relate one of these quantities to the amplitude and frequency of the membrane's vibration. A possible scaling for the velocity is $v \sim \sqrt{gA}$, akin to a fall velocity, which yields the following scaling for the diffusivity:

$$D \sim \sqrt{gA^3}. \tag{3}$$

To test this scaling, we plot the rescaled diffusivity against the rescaled membrane acceleration $\omega^2 A/g$ (Fig. 3). The data points gather along a common relation, which begins where

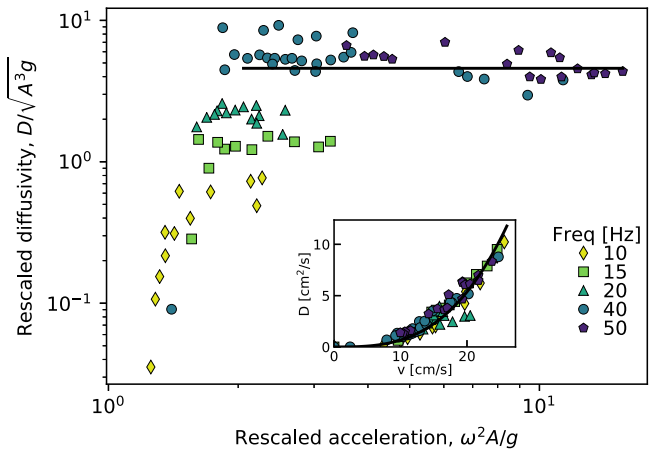

FIG. 3. Rescaled diffusivity as a function of the rescaled acceleration of the membrane. The black line corresponds to Eq. (3). Inset: diffusivity as a function of the grain velocity. The black line corresponds to Eq. (2).

$\omega^2 A \sim g$, and accords with the threshold of bouncing. Then, we observe two distinct regimes, determined by the closeness of the amplitude to the bouncing threshold ($\omega^2 A/g \sim 1$).

Near the threshold ($\omega^2 A/g \lesssim 2$), diffusivity remains low and rapidly increases with acceleration. We suspect that this phenomenon is due to synchronized bouncing [16], wherein the grain's flight duration matches the membrane's vibration period. Avoiding such synchronization requires a large acceleration, particularly at 10 Hz, causing grains to bounce over the ring that corrals them. This explains why the measurements at 10 Hz are confined to the first regime.

Beyond a specific acceleration threshold ($\omega^2 A/g \gtrsim 2$), the diffusivity reaches the scaling of Eq. (3). Consequently, our experiments suggest that the dominant control on the diffusivity is the vibration amplitude and that frequency plays only a secondary role through the threshold of bouncing. This is visible in Fig. 2(c): changing the frequency merely shifts the relation between diffusivity and amplitude. This scaling also suggests that the grain velocity is set by the freefall velocity, with the height typically equal to the vibration amplitude. The proportionality coefficient is $D/\sqrt{gA^3} = 4.6$. This coefficient should also capture the influence of the energy restitution during a collision on the membrane that we maintained constant in our experiments.

In contrast with this observation, Warr *et al.* [17] proposed that velocity scales with the velocity of the vibrating plate of their experiment (ωA), leading to a slope 3 in the Fig. 3, which falls between the two aforementioned regimes. This may originate from a larger acceleration or from the rigidity of the vibrating plate of their experiment.

Overall, this diffusive coefficient is measured here for free grains on a vibrated membrane, as a function of the vibration amplitude, in a previously unexplored configuration. Unlike previous works [9–11], in our system, the grain population is dilute and thus most collisions occur between a grain and the membrane and not between grains themselves ($\rho d^2 < 0.1$). One could also use stochastic force inference to measure the diffusivity, but this method is sensitive to the existence of a ballistic regime [18]. Here, however, the trajectories were abundant enough to guarantee statistical accuracy.

So far, we have established a strong correlation between diffusivity and the vibration amplitude of the membrane. Now,

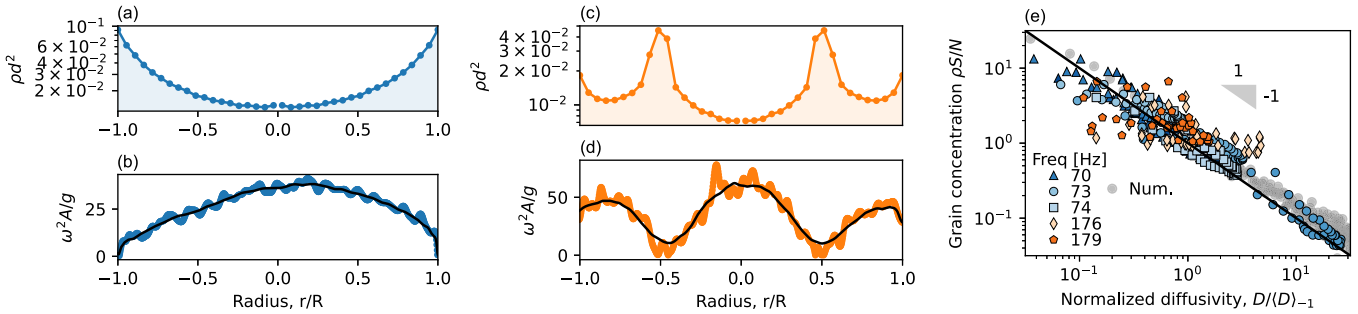

FIG. 4. (a), (b) Mode 1, at 74 Hz. (c), (d) Mode 2, at 179 Hz. (a), (c) Grain concentration as a function of their radial position. (b), (d) Vibration amplitude with Fourier Transform Profilometry. (e) Grain concentration as a function of diffusivity. Equation (4), in black, matches experiments (first and second mode) and numerics (first mode).

when the membrane is excited at resonance, it forms nodes and antinodes [Fig. 1(c)]. The resulting heterogeneity of the vibration amplitude will make diffusivity vary over the membrane. Nodes, which are the loci of a vanishing amplitude, and thus of low diffusivity, coincide with areas of large grain concentration. We now explore the relationship between local diffusivity and grain concentration.

We focus on the first two modes of vibration of the membrane and measure the local grain concentration ρ (Movie 2 in the Supplemental Material). To ensure a sufficient concentration of grains in the antinodes, we increase the total number of grains N, at the cost of accumulating a large density of grains along the nodal lines. We check with the profilometer that this does not affect the vibration of the membrane. Using image analysis to measure the grain concentration, we confirm our expectations: grains cluster along the nodes of vibration, like in Chladni's original experiment. In the first mode, the only nodal line is the edge of the membrane [Figs. 1(e) and 4(a), top], whereas in the second mode, the nodal lines form two concentric circles [Fig. 4(b), top].

We independently measure the local diffusivity through the local vibration amplitude of the membrane, when it is free of grains, using Fourier Transform Profilometry [Fig. 1(a)]. This method consists in projecting fringes onto the surface and correlating their phase with the elevation of the membrane (see the Supplemental Material [19]). This yields the instantaneous elevation of the entire membrane. We then take the absolute value of this elevation and identify the maximum of this quantity with A [Figs. 4(a) and 4(b)]. Finally, as the acceleration $\omega^2 A/g$ significantly exceeds 2, we can confidently apply the scaling provided by Eq. (3) to estimate the diffusivity D.

To correlate diffusivity and grain concentration for all our experiments, we need to normalize the concentration. Assuming this concentration is a power-law function of diffusivity, $\rho \propto D^\alpha$, where α is a real constant, we plot the normalized concentration as a function of the normalized diffusivity, $D/\langle D\rangle_\alpha$, where

$$\langle D\rangle_\alpha = \left(\frac{1}{S}\iint D^\alpha r\, dr\, d\theta\right)^{1/\alpha},$$

with S the membrane's surface. We find that $\alpha = -1$ matches our observations well [Fig. 4(e)] and thus

$$\frac{\rho S}{N} = \frac{\langle D\rangle_{-1}}{D}. \tag{4}$$

To understand this correlation, we must consider the spatial variation of diffusivity. However, how to take into account this variation in the diffusion flux is not obvious [20]. Should the particle flux be $J = -D\nabla\rho$ or $J = -\nabla(D\rho)$—or anything in between [21]? The answer depends on the system, and intermediate cases are also possible [22]. In particular, it depends on where D is to be evaluated: before, during, or after a jump. In our experiments, we expect that the velocity, and consequently the diffusivity, is controlled by the bounce that initiates the parabolic trajectory. Accordingly, following Van Kampen [20], we hypothesize that

$$J = -\nabla(D\rho). \tag{5}$$

At equilibrium, this flux vanishes, which yields after integration $\rho \propto 1/D$. The proportionality coefficient is then such that the integral of the concentration over the entire membrane is N, the total number of particles, which accords with Eq. (4) without fitting parameter over more than two orders of magnitude [Fig. 4(e), black line]. We observe a larger dispersion in the data for the second mode and attribute it to a finite-size effect: the grains jump over a distance comparable to the wavelength of the mode. This dispersion might also originate from a diffusivity regime wherein Eq. (3) does not apply.

To support this interpretation, we conducted numerical simulations of random-walk trajectories with spatially varying step lengths (see Supplemental Material, Sec. V [23]). The data in Fig. 4(e) shows, once again, a remarkable alignment with our model predictions.

Equation (4) means that, in steady state, the concentration of grains is inversely proportional to diffusivity. In other words, grains tend to accumulate where diffusivity is low. This phenomenon provides a sensible explanation for the formation of the Chladni patterns, where nodes coincide with areas of high grain concentration. Alternatively, this distribution could be interpreted as Boltzman's equilibrium, with an *ad hoc* external potential $V = kT\,\log D$, where kT is a temperature [24]. However, our numerical simulations, which involve only statistical effects and no external force, support the present interpretation. The present steady state does not apply to all systems where diffusivity varies; colloidal particles, for instance, distribute themselves uniformly in a close cell, although diffusivity decreases near the walls [25,26]. Unlike our bouncing grains, however, the motion of colloid particles is overdamped, which causes diffusion to take the classical form of Fick's law, $J = -D\nabla\rho$ [27].

In summary, when grains bounce freely over a vibrated surface, they behave as random walkers whose diffusivity depends on the vibration amplitude. If taken into account in the expression of diffusion, this space-dependent diffusivity results in a heterogeneous distribution of grains in steady state, which explains the formation of Chladni patterns. This out-of-equilibrium system represents an elementary form of active matter, wherein individual particles constantly extract energy from areas of intense vibration and transfer it to quieter areas [28–30]. Despite its simplicity, this system shows a remarkably consistent, and nontrivial, macroscopic behavior.

In the future, investigating the system's dynamics should be possible. Based on expression (5), the mass balance for the grains reads $\partial_t \rho = \Delta(D\rho)$. As a preliminary investigation, we started an experiment with a uniform grain concentration. Despite reproducibility challenges, we estimated a characteristic relaxation time of $\tau = 5 \pm 2$ s, close to the expected $\tau \sim D^2/R$, given $R \sim 10$ cm and $D = 1$–10 cm^2/s.

Finally, other configurations could lead to space-dependent diffusion. For example, tuning the elasticity coefficient of the membrane, upon which the grains bounce, should also induce spatial variations in the grain concentration [31].

We are indebted to P. Szymczak and P. Popović for stimulating and illuminating discussions on the subject. We also warmly thank A. Eddi and P. Cobelli for their help on the Fourier Transform Profilometry technique.

[1] M. Faraday, XVII. on a peculiar class of acoustical figures; and on certain forms assumed by groups of particles upon vibrating elastic surfaces, Philos. Trans. R. Soc. London **121**, 299 (1831).
[2] A. Okuda and T. Ono, Bracing effect in a guitar top board by vibration experiment and modal analysis, Acoust. Sci. Tech. **29**, 103 (2008).
[3] Y. Liu, Q. Yin, Y. Luo, Z. Huang, Q. Cheng, W. Zhang, B. Zhou, Y. Zhou, and Z. Ma, Manipulation with sound and vibration: A review on the micromanipulation system based on sub-MHz acoustic waves, Ultrasonics Sonochem. **96**, 106441 (2023).
[4] G. Vuillermet, P.-Y. Gires, F. Casset, and C. Poulain, Chladni patterns in a liquid at microscale, Phys. Rev. Lett. **116**, 184501 (2016).
[5] H. J. van Gerner, M. A. van der Hoef, D. van der Meer, and K. van der Weele, Inversion of chladni patterns by tuning the vibrational acceleration, Phys. Rev. E **82**, 012301 (2010).
[6] H. J. van Gerner, K. van der Weele, M. A. van der Hoef, and D. van der Meer, Air-induced inverse chladni patterns, J. Fluid Mech. **689**, 203 (2011).
[7] K.-F. Bohringer, V. Bhatt, and K. Y. Goldberg, Sensorless manipulation using transverse vibrations of a plate, in *Proceedings of 1995 IEEE International Conference on Robotics and Automation* (IEEE, New York, 1995), Vol. 2, pp. 1989–1996.
[8] J. Arango and C. Reyes, Stochastic models for chladni figures, Proc. Edinburgh Math. Soc. **59**, 287 (2016).
[9] H. M. Jaeger, S. R. Nagel, and R. P. Behringer, Granular solids, liquids, and gases, Rev. Mod. Phys. **68**, 1259 (1996).
[10] R. D. Wildman, J. M. Huntley, and J.-P. Hansen, Self-diffusion of grains in a two-dimensional vibrofluidized bed, Phys. Rev. E **60**, 7066 (1999).
[11] P. Melby, F. V. Reyes, A. Prevost, R. Robertson, P. Kumar, D. A. Egolf, and J. S. Urbach, The dynamics of thin vibrated granular layers, J. Phys.: Condens. Matter **17**, S2689 (2005).
[12] I. Grabec, Vibration driven random walk in a chladni experiment, Phys. Lett. A **381**, 59 (2017).
[13] L. Gosnet, A. Abramian, S. Protiére, and A. Lazarus, Mesure de la tension d'une membrane à l'aide des figures de Chladni, Bull l'Union Phys. **117**, 519 (2023).
[14] The library can be found on https://github.com/odevauchelle/BrownTrack.
[15] J. Tailleur and M. E. Cates, Statistical mechanics of interacting run-and-tumble bacteria, Phys. Rev. Lett. **100**, 218103 (2008).
[16] J.-Y. Chastaing, E. Bertin, and J.-C. Géminard, Dynamics of a bouncing ball, Am. J. Phys. **83**, 518 (2015).
[17] S. Warr, W. Cooke, R. Ball, and J. Huntley, Probability distribution functions for a single-particle vibrating in one dimension: experimental study and theoretical analysis, Physica A **231**, 551 (1996).
[18] A. Frishman and P. Ronceray, Learning force fields from stochastic trajectories, Phys. Rev. X **10**, 021009 (2020).
[19] See Supplemental Material at http://link.aps.org/supplemental/10.1103/PhysRevResearch.7.L032001 for a detailed description of the experimental and numerical methods.
[20] N. Van Kampen, Diffusion in inhomogeneous media, J. Phys. Chem. Solids **49**, 673 (1988).
[21] M. J. Schnitzer, Theory of continuum random walks and application to chemotaxis, Phys. Rev. E **48**, 2553 (1993).
[22] A. W. C. Lau and T. C. Lubensky, State-dependent diffusion: Thermodynamic consistency and its path integral formulation, Phys. Rev. E **76**, 011123 (2007).
[23] I. Grabec and N. Sok, Diffusion equation generalized for modeling of chladni patterns, Strojniški vestnik-J. Mech. Eng. **69**, 284 (2023).
[24] J. Hunter, P. Craig, and H. Phillips, On the use of random walk models with spatially variable diffusivity, J. Comput. Phys. **106**, 366 (1993).
[25] L. P. Faucheux and A. J. Libchaber, Confined brownian motion, Phys. Rev. E **49**, 5158 (1994).
[26] J. Agudo-Canalejo, T. Adeleke-Larodo, P. Illien, and R. Golestanian, Enhanced diffusion and chemotaxis at the nanoscale, Acc. Chem. Res. **51**, 2365 (2018).
[27] This subtlety was pointed out by P. Szymczak.
[28] A. Kudrolli, G. Lumay, D. Volfson, and L. S. Tsimring, Swarming and swirling in self-propelled polar granular rods, Phys. Rev. Lett. **100**, 058001 (2008).
[29] J. Deseigne, O. Dauchot, and H. Chaté, Collective motion of vibrated polar disks, Phys. Rev. Lett. **105**, 098001 (2010).
[30] As noted by P. Popović (private communication).
[31] O. Devauchelle, P. Popovi, P. Szymczak, A. Abramian, and A. Lazarus, A granular Büttiker-Landauer motor (unpublished).